eliminates force-generation and keeps this site buried.

Differential labeling in MSCs is also found at the single Cys site of vimentin (Fig. 4D): Cys^{327} is in the central coil that mediates coiled-coil polymerization (35). Quaternary structure changes in solution have been exploited previously to understand hemoglobin tetramerization [e.g., (36)], as well as actin-binding interfaces [e.g., (37)], and here blebbistatin-induced depolymerization of vimentin with Cys exposure in the MSCs appears consistent with blebbistatin-induced softening of the cells (32). Purified vimentin confirms enhanced labeling as monomer (~50% more) versus polymer (Fig. 4D), and Western blot analysis plus immunofluorescence imaging of MSCs grown on various matrices show that chronic blebbistatin treatment consistently down-regulates vimentin (fig. S4, B and C). Short treatments with blebbistatin (~1 hour instead of 1 day) also show that mBBr-vimentin measured in cell lysates increases significantly even though Western blots and immunofluorescence indicate no differences in overall expression. In-cell labeling thus identifies structural changes within tensed cell but not relaxing cells.

Nucleated cells typified by MSCs have a complex intracellular force map when inferred from cell tractions in the surrounding matrix (4, 32, 38), and even simple cells such as RBCs sustain stresses at the molecular level in unknown ways (1, 29). The overall Cys-shotgun methodology here not only provides evidence of force-induced changes that propagate in both tertiary and quaternary structures within cells but also, through LC-MS/MS, provides useful proteomic information, as well as new opportunities for fluorescence imaging. In addition, whereas fluorescence resonance energy–transfer imaging of labeled proteins within cells [e.g., (39)] might allow imaging of force-induced conformational changes in real time, the time-integrated analyses here are complementary and also readily extended to engineered sites in wild-type and mutant proteins for in-cell assessments of perturbations. This idea seems very likely to extend to coincidence detection of Cys labeling with posttranslational events such as phosphorylation so as to precisely colocalize conformational changes with signaling events.

References and Notes
1. E. A. Evans, R. Skalak, *Mechanics and Thermodynamics of Biomembranes* (CRC Press, Boca Raton, FL, 1980), p. 190.
2. H. P. Erickson, *Proc. Natl. Acad. Sci. U.S.A.* **91**, 10114 (1994).
3. N. Q. Balaban *et al.*, *Nat. Cell Biol.* **3**, 466 (2001).
4. K. A. Beningo, M. Dembo, I. Kaverina, J. V. Small, Y. L. Wang, *J. Cell Biol.* **153**, 881 (2001).
5. F. J. Alenghat, D. E. Ingber, *Sci. STKE* **2002** (119), PE6 (2002).
6. E. A. Evans, D. A. Calderwood, *Science* **316**, 1148 (2007).
7. V. Vogel, M. Sheetz, *Nat. Rev. Mol. Cell Biol.* **7**, 265 (2006).
8. A. Bershadsky, M. Kozlov, B. Geiger, *Curr. Opin. Cell Biol.* **18**, 472 (2006).
9. M. Rief, M. Gautel, F. Oesterhelt, J. M. Fernandez, H. E. Gaub, *Science* **276**, 1109 (1997).
10. A. F. Oberhauser, P. E. Marszalek, H. P. Erickson, J. M. Fernandez, *Nature* **393**, 181 (1998).
11. I. Schwaiger, C. Sattler, D. R. Hostetter, M. Rief, *Nat. Mater.* **1**, 232 (2002).
12. G. Lee *et al.*, *Nature* **440**, 246 (2006).
13. M. Sotomayor, K. Schulten, *Science* **316**, 1144 (2007).
14. P. M. Williams *et al.*, *Nature* **422**, 446 (2003).
15. V. Ortiz, S. O. Nielsen, M. L. Klein, D. E. Discher, *J. Mol. Biol.* **349**, 638 (2005).
16. N. I. Abu-Lail, T. Ohashi, R. L. Clark, H. P. Erickson, S. Zauscher, *Matrix Biol.* **25**, 175 (2006).
17. Y. Sawada *et al.*, *Cell* **127**, 1015 (2006).
18. J. H. Ha, S. N. Loh, *Nat. Struct. Biol.* **5**, 730 (1998).
19. J. A. Silverman, P. B. Harbury, *J. Biol. Chem.* **277**, 30968 (2002).
20. C. P. Johnson *et al.*, *Blood* **109**, 3538 (2007).
21. P. Carl, C. H. Kwok, G. Manderson, D. W. Speicher, D. E. Discher, *Proc. Natl. Acad. Sci. U.S.A.* **98**, 1565 (2001).
22. A. P. Wiita, S. R. Ainavarapu, H. H. Huang, J. M. Fernandez, *Proc. Natl. Acad. Sci. U.S.A.* **103**, 7222 (2006).
23. Materials and methods are available as supporting material on *Science* Online.
24. N. Mohandas, E. A. Evans, *Annu. Rev. Biophys. Biomol. Struct.* **23**, 787 (1994).
25. M. Rief, J. Pascual, M. Saraste, H. E. Gaub, *J. Mol. Biol.* **286**, 553 (1999).
26. R. Law *et al.*, *Biophys. J.* **85**, 3286 (2003).
27. L. G. Randles, R. W. Rounsevell, J. Clarke, *Biophys. J.* **92**, 571 (2007).
28. H. Kusunoki, R. I. MacDonald, A. Mondragon, *Structure* **12**, 645 (2004).
29. X. An *et al.*, *J. Biol. Chem.* **281**, 10527 (2006).
30. J. C. Lee, D. E. Discher, *Biophys. J.* **81**, 3178 (2001).
31. R. McBeath, D. M. Pirone, C. M. Nelson, K. Bhadriraju, C. S. Chen, *Dev. Cell* **6**, 483 (2004).
32. A. J. Engler, S. Sen, H. L. Sweeney, D. E. Discher, *Cell* **126**, 677 (2006).
33. A. F. Straight *et al.*, *Science* **299**, 1743 (2003).
34. B. Ramamurthy, C. M. Yengo, A. F. Straight, T. J. Mitchison, H. L. Sweeney, *Biochemistry* **43**, 14832 (2004).
35. H. Herrmann, U. Aebi, *Annu. Rev. Biochem.* **73**, 749 (2004).
36. E. Chiancone, D. L. Currell, P. Vecchini, E. Antonini, J. Wyman, *J. Biol. Chem.* **245**, 4105 (1970).
37. S. Sun, M. Footer, P. Matsudaira, *Mol. Biol. Cell* **8**, 421 (1997).
38. N. Wang *et al.*, *Am. J. Physiol. Cell Physiol.* **282**, C606 (2002).
39. V. S. Kraynov *et al.*, *Science* **290**, 333 (2000).
40. We thank V. Ortiz for the Molecular Dynamics image, X. An for purified protein, A. Engler for culture and help with MSCs, and A. Kashina for helpful comments on the manuscript. We gratefully acknowledge support from NIH grants (D.E.D., D.W.S.), NIH Training Grants (C.P.J., C.C.), as well as NSF and Muscular Dystrophy Association grants (D.E.D.).

Monitoring of Blood Vessels and Tissues by a Population of Monocytes with Patrolling Behavior

Cedric Auffray,[1] Darin Fogg,[1] Meriem Garfa,[1] Gaelle Elain,[1] Olivier Join-Lambert,[2,3] Samer Kayal,[1,2,3] Sabine Sarnacki,[2,3] Ana Cumano,[4] Gregoire Lauvau,[5] Frederic Geissmann[1,2,3]*

The cellular immune response to tissue damage and infection requires the recruitment of blood leukocytes. This process is mediated through a classical multistep mechanism, which involves transient rolling on the endothelium and recognition of inflammation followed by extravasation. We have shown, by direct examination of blood monocyte functions in vivo, that a subset of monocytes patrols healthy tissues through long-range crawling on the resting endothelium. This patrolling behavior depended on the integrin LFA-1 and the chemokine receptor CX_3CR1 and was required for rapid tissue invasion at the site of an infection by this "resident" monocyte population, which initiated an early immune response and differentiated into macrophages.

Mammalian monocytes consist of two main subsets of immune cells (1, 2), which arise from a common hematopoietic progenitor, the macrophage and dendritic cell (DC) precursor (MDP, or monoblast) that also gives rise to conventional resident spleen DCs (cDCs) and several tissue macrophage subsets (3, 4). So-called "inflammatory" monocytes express the cell surface protein Ly6c ($Gr1^+$), the chemokine receptor CCR2, and the adhesion molecule L-selectin and are selectively recruited to inflamed tissues and lymph nodes (1, 5). They are able to differentiate into inflammatory DC (1, 6, 7) and can replenish resident cell compartments in the skin, digestive tract, and lung (3, 8). The second subset of monocytes has been termed "resident" in mice (1, 2) because they were found in both resting and inflamed tissues, although their functions are still unknown. This subset is defined by a smaller size, high expression of the chemokine receptor CX_3CR1 and LFA-1 integrin, and by the lack of expression of Ly6c ($Gr1^-$), CCR2, and L-selectin (1, 2). Two monocyte subsets can also be identified in humans (9), with $CD14^+$ $CD16^-$ monocytes resembling mouse inflammatory monocytes and $CD14^{low}$ $CD16^+$ monocytes sharing a phenotype similar to that of mouse resident monocytes (1). Resident and

inflammatory monocytes thus appear to be defined by distinct sets of adhesion molecules and chemokine receptors, which suggests different modes of tissue trafficking.

To explore this possibility further, we developed a strategy to study the behavior and functions of blood monocytes, in real time, under steady state or inflammatory conditions. Intravital confocal microscopy imaging was undertaken in vivo in a way that allowed us to observe cells within capillaries and postcapillary vessels in the dermis (Fig. 1A) and in larger veins and arteries, that is, mesenteric vessels (Fig. 1B) (10). $Cx_3cr1^{gfp/+}$ mice, which express green fluorescent protein (GFP) in monocytes [but also in natural killer (NK) cells and some T cells] and $Rag_2^{-/-}$, $\gamma_c^{-/-}$, $Cx_3cr1^{gfp/+}$ mice, in which monocytes are the only blood cells expressing GFP, were used as reporters (Fig. 1, C and D) (10).

Intravital microscopy observation of tissues in the steady state revealed that monocytes within most blood vessels in the dermis (Fig. 2, A and B, and movies S1 and S2) and in the branches of the mesenteric vein and the mesenteric artery (Fig. 2C, fig. S1, and movies S3 and S4) exhibited a constitutive "crawling" type motility. In contrast,

rolling gfp$^+$ monocytes were observed only transiently after surgery in the mesenteric veins (fig. S1 and movies S3 and S4) but not in arteries (movie S4). Analysis of gfp signal intensity per pixel indicated that crawling monocytes belonged predominantly to the gfp^{high} subset (CX$_3$CR1^{high} Gr1$^-$) as compared with monocytes that perform rolling in the same vessels (Fig. 2D and fig. S2). These finding suggested either that gfp^{high} monocytes were crawling inside blood vessels onto endothelial cells, despite the blood flow, or that they were located outside the lumen of the blood vessel. When the green gfp signal was omitted, crawling gfp^{high} monocytes appeared as dark spots on confocal sections of the vessel labeled in red with the fluorescent dextran, indicating that monocytes are located inside the blood vessels (Fig. 2E and movie S5). Crawling polymorphonuclear neutrophils (PMN) or lymphocytes would appear as dark crawling cells in the blood of mice; however, gfp$^-$ crawling cells were not observed in the steady state (movie S1), suggesting that these cells did not behave in the same way and that gfp$^+$ monocytes were the majority of cells that crawl on the endothelium in the steady state.

Although monocytes were located inside the vessels, overlay of individual cell tracks plotted after aligning their starting positions indicated that the direction of their crawling movement was not dependent on the blood flow (Fig. 2F). Extravasation was rarely observed in the steady state. The path of individual cells indicated that monocytes in blood vessels appeared to describe loops (25%), hairpin (17%), waves (38%), mixed pattern (9%), and short path (<40 µm, 11%) (Fig. 2, G to J, and fig. S3). The average instantaneous velocity of crawling monocytes was 4

to 20 µm/min (average 12 µm/min) (Fig. 2K and fig. S4). The distance traveled by individual cells was, on average, only half their path length, indicating that the cells have a high confinement ratio (Fig. 2L). The result of these crawling movements was that in small postcapillary venules, after an hour, monocytes appeared to have extensively monitored the endothelium of a given vessel (Fig. 2B and movie S2), leading us to describe their behavior as patrolling.

The velocity profile of flow in blood vessels is generally parabolic across the cross section of the vessel, and calculated values decrease to zero at the blood vessel wall (11). However, crawling against the midstream blood flow is counterintuitive, and this suggested that monocytes were closely adherent to the luminal side of the endothelium. We therefore explored the molecular basis of monocyte patrolling. Lymphocytes and PMNs have been shown to roll at speeds of ~40 µm/sec under conditions of flow at sites of inflammation along the endothelium of postcapillary venules (12, 13). This initial contact allows endothelial membrane-bound chemokines to activate leukocyte integrins through $G\alpha_i$-linked chemokine receptor (14). Changes in integrin affinity then allow the rolling leukocytes to stick firmly, occasionally crawl onto the endothelial cell toward the closest intracellular cell junction (15, 16), and diapedese across the endothelium. Patrolling was slower than rolling by a factor of 100 to 1000 and was observed in the steady state, long-range, and independent of the direction of midstream blood flow and of extravasation. However, it appears to involve a "firm binding" to endothelium, and therefore we reasoned that integrin may be involved. Gfp^{high} (Gr1$^-$) monocytes express the β_2 integrins LFA-1

[1]Institut Nationale de la Santé et de la Recherche Médicale (INSERM) U838, Laboratory of Biology of the Mononuclear Phagocyte System, and Cellular and Molecular imaging core facility, Institut Fédératif de Recherche Necker-Enfants Malades, Paris, France. [2]University Paris-Descartes, Paris, France. [3]Hôpital Necker-Enfants Malades, AP-HP, Paris, France. [4]INSERM U668, Unité de Développement des Lymphocytes, Institut Pasteur, Paris, France. [5]INSERM E03-44, Institut de Pharmacologie Moleculaire et Cellulaire, Nice, France.

*To whom correspondence should be addressed. E-mail: geissmann@necker.fr

Fig. 1. Intravital imaging of mouse monocytes. (**A**) CX$_3$CR1-expressing cells express gfp in reporter mice, and dermal blood vessels are labeled in red rhodamine-conjugated dextran. (**B**) The branches of the mesenteric vein (arrowhead) and mesenteric artery (arrow) are surgically exposed. (**C**) Flow cytometry analysis of blood leukocytes from $Cx_3cr1^{gfp/+}$ mice, $Rag_2^{-/-}$ $Cx_3cr1^{gfp/+}$ mice $Rag_2^{-/-}$, $\gamma_c^{-/-}$ $Cx_3cr1^{gfp/+}$ mice, and $Rag_2^{-/-}$, $\gamma_c^{-/-}$, $Cx_3cr1^{gfp/+}$ mice reconstituted with wild-type lymphoid cells. (**D**) Gr1$^+$ (gfp^{low}) and Gr1$^-$ (gfp^{high}) monocytes were sorted by flow cytometry and examined by confocal microscopy. Based on gfp intensity, Gr1$^-$ (gfp^{high}) monocytes sorted by fluorescence-activated cell sorting (FACS) are easily distinguishable by confocal microscopy from FACS-sorted Gr1$^+$ (gfp^{low}) monocytes labeled with a far-red cell tracker (shown in blue in the middle panel).
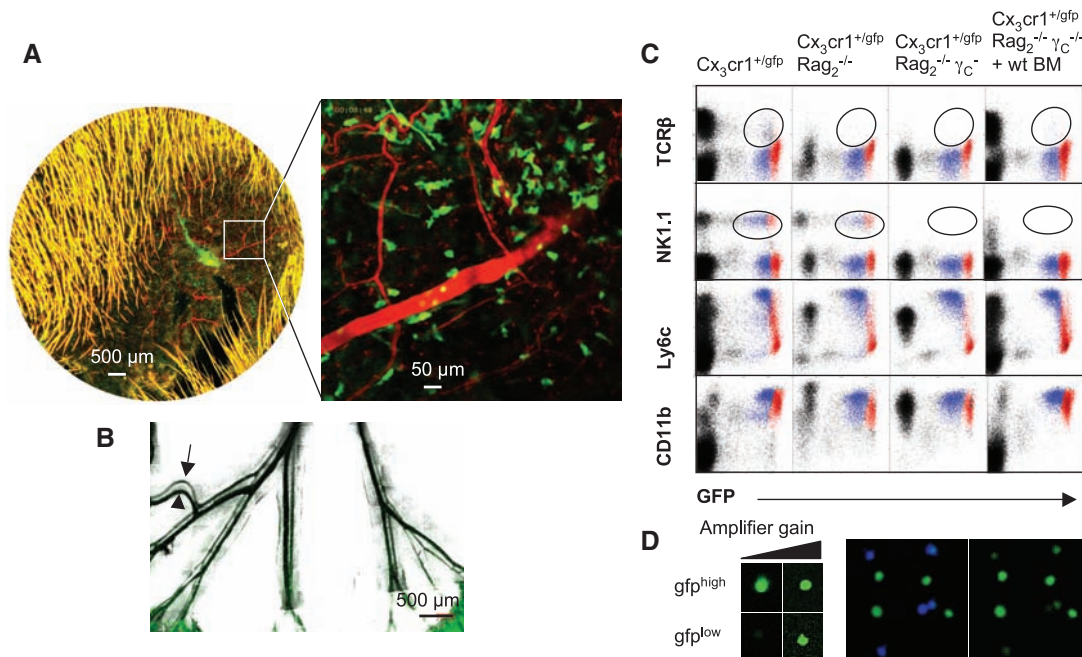
(CD11a/CD18, $\alpha_L\beta_2$) and Mac-1 (CD11b/CD18, $\alpha_M\beta_2$) (*1*). Intravenous injection of blocking antibodies to either CD11a or CD18, but not of antibodies to CD11b or control immunoglobulin (Ig), resulted in the rapid, complete, and prolonged release of monocytes from the endothelial wall (Fig. 3, A and B, and movie S6), indicating that LFA-1 is required for crawling. Gfp^{high} monocytes also express high levels of the chemokine receptor CX$_3$CR1 (*1*), whereas its ligand, Fractalkine, is a transmembrane molecule exp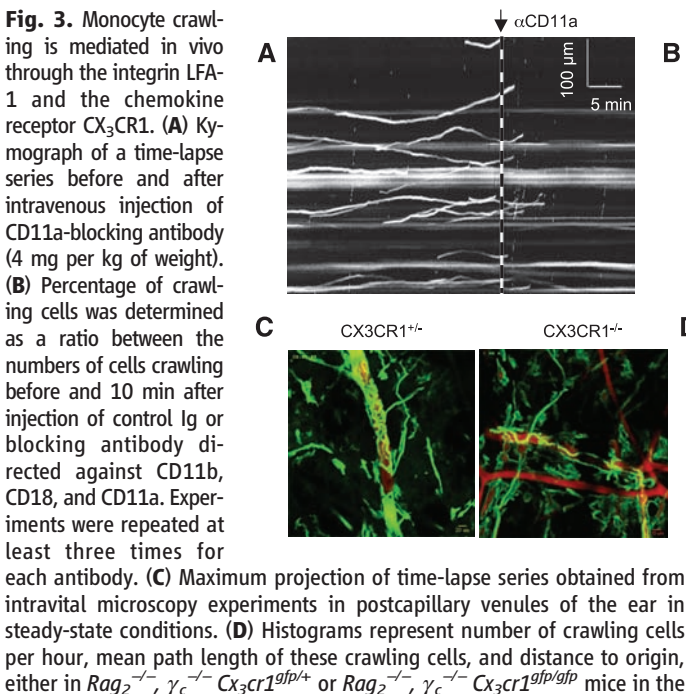ressed on endothelial cells (*17–19*). CX$_3$CR1- fractalkine interaction in vitro has been described to mediate adhesion between monocytes and endothelial cells through activation of integrins (*20*) and through an intrinsic adhesion function (*18, 20, 21*). The number of crawling monocytes was reduced by two-thirds in CX$_3$CR1-deficient

Fig. 2. Gfp^{high} Gr1$^-$ monocytes crawl inside blood vessels. (**A**) Dermal blood vessels in *Rag$_2$$^{-/-}$, $\gamma_c$$^{-/-}$ Cx$_3$cr1$^{gfp/+}$* reporter mice. Monocytes appear as green dots (arrows). (**B** and **C**) Green signal from images of time-lapse series are summed to display the path of labeled cells in the dermis (B) and mesenteric vessels (C). In (C), the open arrow indicates a branch of the mesenteric vein, and the closed arrow indicates a branch of the mesenteric artery. (**D**) gfp maximal pixel intensity was calculated as indicated in fig. S2. (**E**) Confocal section (6 μm) examined with red (intravenous dextran) and green (gfp$^+$ monocytes) signals, or for the red signal only (shown in gray, right panel). Cells that are located within the vessels appear as a dark signal (arrow). (**F**) Overlay of monocyte tracks from two representative vessels, plotted after aligning their starting positions. (**G** to **I**) Path (G), kymograph (H), and instantaneous velocity (I) of a cell from movie S1. (**J**) Monocyte paths were classified as loops, hairpin, waves, mixed pattern, and short path (<40 μm) (fig. S3). (**K**) Average velocity was calculated as indicated in (*10*). (**L**) Confinement ratio of gfp^{high} monocytes. Scatter plot represents the ratio of the distance to origin of tracked cells versus their path length.

Fig. 3. Monocyte crawling is mediated in vivo through the integrin LFA-1 and the chemokine receptor CX$_3$CR1. (**A**) Kymograph of a time-lapse series before and after intravenous injection of CD11a-blocking antibody (4 mg per kg of weight). (**B**) Percentage of crawling cells was determined as a ratio between the numbers of cells crawling before and 10 min after injection of control Ig or blocking antibody directed against CD11b, CD18, and CD11a. Experiments were repeated at least three times for each antibody. (**C**) Maximum projection of time-lapse series obtained from intravital microscopy experiments in postcapillary venules of the ear in steady-state conditions. (**D**) Histograms represent number of crawling cells per hour, mean path length of these crawling cells, and distance to origin, either in *Rag$_2$$^{-/-}$, $\gamma_c$$^{-/-}$ Cx$_3$cr1$^{gfp/+}$* or *Rag$_2$$^{-/-}$, $\gamma_c$$^{-/-}$ Cx$_3$cr1$^{gfp/gfp}$* mice in the steady state. (**E**) Histograms represent number of Gr1$^-$ monocytes in the blood of 10-week-old *Rag$_2$$^{-/-}$, $\gamma_c$$^{-/-}$ Cx$_3$cr1$^{gfp/+}$* and *Rag$_2$$^{-/-}$, $\gamma_c$$^{-/-}$ Cx$_3$cr1$^{gfp/gfp}$* mice. (**F**) Representation of the crawling velocity of Gr1$^-$ monocytes from *Rag$_2$$^{-/-}$, $\gamma_c$$^{-/-}$ Cx$_3$cr1$^{gfp/+}$* (solid line) and *Rag$_2$$^{-/-}$, $\gamma_c$$^{-/-}$ Cx$_3$cr1$^{gfp/gfp}$* (dashed line) mice.

mice, and the average path length of crawling cells was reduced by one-half, resulting in a six-fold decrease in patrolling (Fig. 3, C and D, and movie S7), whereas the velocity of the remaining crawling monocytes and the numbers of circulating blood gfp^{high} monocytes were similar in $Cx_3cr1^{-/-}$ and $Cx_3cr1^{+/-}$ mice (Fig. 3, E and F, and fig. S5). It is notable that blocking antibodies to LFA-1 can detach crawling monocytes in $Cx_3cr1^{+/-}$ mice, which suggests that CX$_3$CR1-dependent crawling is largely mediated through LFA-1 in vivo.

The patrolling monocytes are ideally located to provide immune surveillance of endothelial cells and surrounding tissues. In response to tissue damage, gfp^{high} monocytes extravasated rapidly within 1 hour and invaded the surrounding tissues after exposure to irritants (Fig. 4, A and B), aseptic wounding (Fig. 4C), and peritoneal infection with *Listeria monocytogenes* (Fig. 4D). To study in depth the kinetics, phenotype, and functions of extravasated monocytes, we used the *L. monocytogenes* peritoneal infection model, because extravasated cells can easily be recovered by peritoneal lavage. In this model, extravasation of Gr1$^-$ gfp^{high} monocytes peaked at 2 hours after infection, at a time when PMN is only beginning to enter the peritoneum and several hours before the extravasation of conventional Gr1$^+$ gfp^{low} monocytes is observed, and was significantly delayed in patrolling-deficient $Cx3cr1^{-/-}$ mice (Fig. 4D and table S1). Therefore, patrolling was associated with, and required for, early extravasation and tissue invasion by Gr1$^-$ gfp^{high} monocytes. Extravasated Gr1$^-$ gfp^{high} monocytes were responsible for an early inflammatory response (Fig. 4, E and F, and fig. S6). At 1 and 2 hours after infection, Gr1$^-$ gfp^{high} monocytes were the only producers of tumor necrosis factor–α (TNFα), a cytokine central to inflammation, as detected by intracellular flow cytometry and polymerase chain reaction (PCR) (Fig. 4F). Genes coding for interleukin-1 (IL-1), lysozyme, defensins, complement, pattern recognition receptors such as TLRs, scavenger receptors, and IgFc receptors, and chemokines involved in the recruitment and activation of other effector cells were also up-regulated (Fig. 4E and fig. S6).

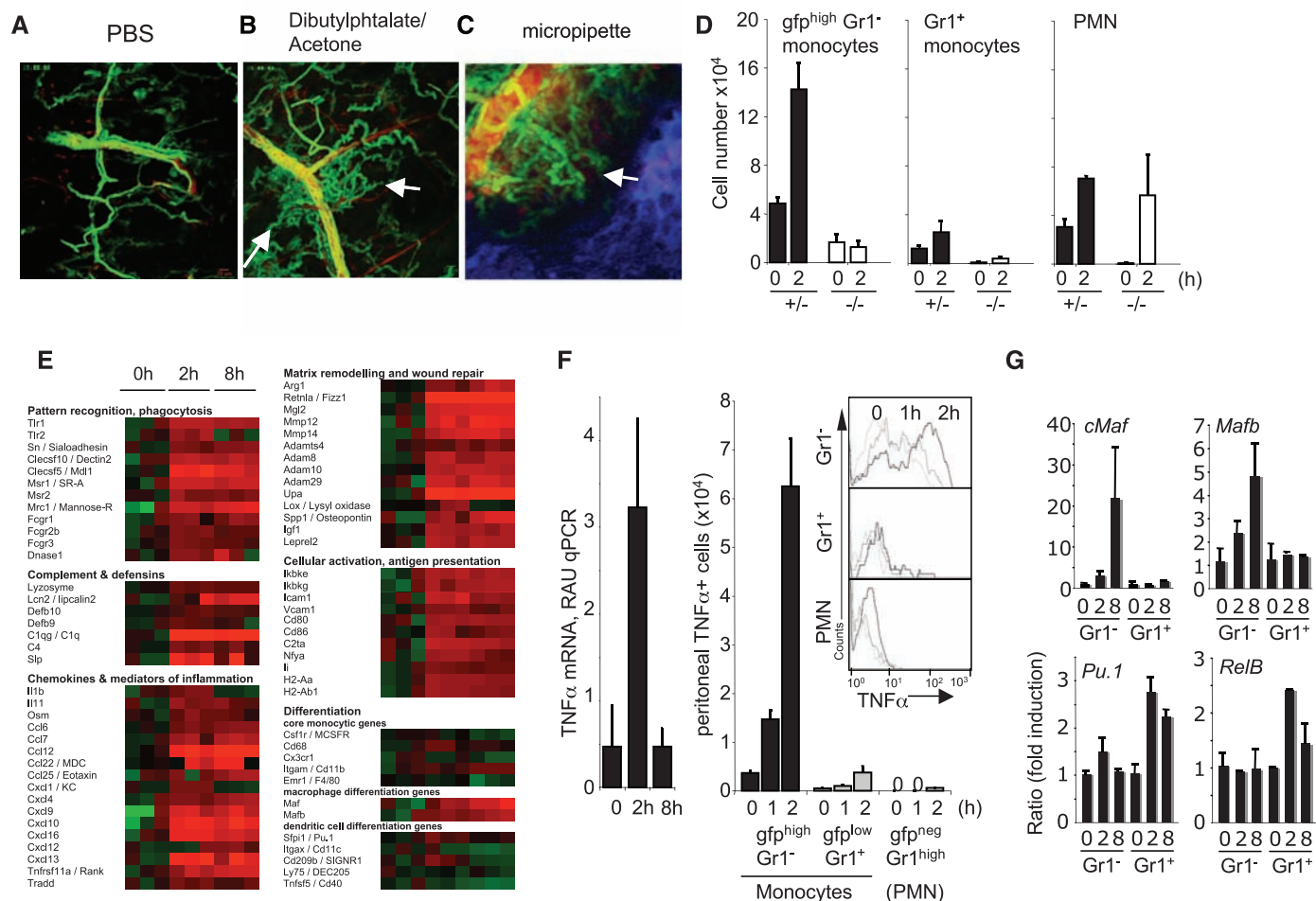Notably, the production of TNF and IL-1 was transient and turned off at 8 hours (Fig. 4F),

Fig. 4. Rapid tissue invasion by patrolling Gfp^{high} Gr1$^-$ monocytes after tissue damage or infection. (**A** to **C**) Crawling gfp^{high} monocytes in the mouse dermis are tracked for 1 hour after application of phosphate-buffered saline (PBS) (A) or 1:1 dibutylphtalate acetone (B), or after aseptic damage with a microinjection pipette loaded with a far-red dye (shown in blue) (C). (**D**) Number of extravasated cells recovered from the peritoneal cavity of mice infected with *L. monocytogenes*. (**E**) Analysis of gene expression on purified GFP^{high} monocytes (fig. S6) (*10*). (**F**) GFP^{high} monocytes recovered from the peritoneum of infected mice are the main producers of TNFα in vivo at 2 hours after *L. monocytogenes* infection. (Data are mean ± SD; n = 3 in each group; representative experiment out of four). (**G**) Extravasated Gr1$^-$ gfp^{high} monocytes initiated a macrophage differentiation program, at the expense of DC differentiation, whereas Gr1$^+$ gfp^{low} monocytes initiated a DC differentiation program. Regulation of Mafb, cMaf, Pu.1, and RelB genes was analyzed as described in figs. S6 and S7.

whereas extravasated Gr1⁻ gfp^high monocytes turned on—at 2 and 8 hours—genes involved in tissue remodeling (22), including arginase1, Fizz1, Mgl2, and mannose receptor (MR) (Fig. 4E and fig. S9).

Indeed, the study of the balance of transcription factors that specifies the alternative macrophage or dendritic cell fate of monocytes (23) indicated that extravasated Gr1⁻ gfp^high monocytes initiated a typical macrophage differentiation program, characterized by up-regulation of cMaf and MafB but not RelB and Pu.1 (sfpi1) (Fig. 4G and figs. S6 and S7). In contrast, the conventional Gr1⁺ gfp^low monocytes initiated a DC differentiation program, as described previously (1, 6), by up-regulating RelB and Pu.1 but not cMaf and MafB (Fig. 4G and fig. S6). Analysis of the expression of a larger panel of genes differentially regulated in monocyte-derived macrophages and DC supported this conclusion (fig. S8).

These findings demonstrate a new mechanism of leukocyte crawling on endothelial cells and a new role for LFA-1. The present data also assign a function to gfp^high Gr1⁻ monocytes. Patrolling of blood vessels by these resident monocytes allow rapid tissue invasion by monocytes in case of damage and infection, followed by the initiation of an innate immune response and their differentiation into macrophages. This is in contrast to the role of Gr1⁺ monocytes, which reach the inflammatory site later and give rise to inflammatory DCs (1, 6). This reveals an unsuspected dichotomy of the differentiation potential and functions of blood monocyte subsets during infection. The extravasation of patrolling Gr1⁻ gfp^high monocytes is likely to be dependent on a yet-unidentified signal(s) from damaged tissue and/or endothelium. Interestingly, the existence of a pool of "marginated" monocytes expressing CD16⁺ has been proposed in humans (24) and may correspond, at least in part, to the patrolling behavior that we describe here, suggesting a similar in vivo function of mouse resident CX₃CR1^high (gfp^high) Gr1^low monocytes and human CX₃CR1^high CD16⁺ CD14^low monocytes. Monocytes are abundant in arthritis and atherosclerotic lesions (25, 26), and CX₃CR1, TNF-α, and LFA-1 have been implicated in the pathogenesis of these inflammatory diseases (27, 28); thus, patrolling monocytes may contribute to their pathogenesis and may represent a target for treatment.

References and Notes

1. F. Geissmann, S. Jung, D. R. Littman, *Immunity* **19**, 71 (2003).
2. C. Sunderkotter et al., *J. Immunol.* **172**, 4410 (2004).
3. C. Varol et al., *J. Exp. Med.* **204**, 171 (2007).
4. D. K. Fogg et al., *Science* **311**, 83 (2006).
5. R. T. Palframan et al., *J. Exp. Med.* **194**, 1361 (2001).
6. N. V. Serbina, T. P. Salazar-Mather, C. A. Biron, W. A. Kuziel, E. G. Pamer, *Immunity* **19**, 59 (2003).
7. S. H. Naik et al., *Nat. Immunol.* **7**, 663 (2006).
8. F. Ginhoux et al., *Nat. Immunol.* **7**, 265 (2006).
9. B. Passlick, D. Flieger, H. W. Ziegler-Heitbrock, *Blood* **74**, 2527 (1989).
10. Materials and methods are available as supporting material on *Science* Online.
11. M. L. Smith, D. S. Long, E. R. Damiano, K. Ley, *Biophys. J.* **85**, 637 (2003).
12. T. A. Springer, *Cell* **76**, 301 (1994).
13. A. Fischer, B. Lisowska-Grospierre, D. C. Anderson, T. A. Springer, *Immunodefic. Rev.* **1**, 39 (1988).
14. G. Constantin et al., *Immunity* **13**, 759 (2000).
15. M. Phillipson et al., *J. Exp. Med.* **203**, 2569 (2006).
16. A. R. Schenkel, Z. Mamdouh, W. A. Muller, *Nat. Immunol.* **5**, 393 (2004).
17. J. F. Bazan et al., *Nature* **385**, 640 (1997).
18. A. M. Fong et al., *J. Exp. Med.* **188**, 1413 (1998).
19. T. Imai et al., *Cell* **91**, 521 (1997).
20. S. Goda et al., *J. Immunol.* **164**, 4313 (2000).
21. C. A. Haskell, M. D. Cleary, I. F. Charo, *J. Biol. Chem.* **275**, 34183 (2000).
22. G. H. Ghassabeh et al., *Blood* **108**, 575 (2006).
23. Y. Bakri et al., *Blood* **105**, 2707 (2005).
24. B. Steppich et al., *Am. J. Physiol. Cell Physiol.* **279**, C578 (2000).
25. M. Iwahashi et al., *Arthritis Rheum.* **50**, 1457 (2004).
26. A. Schlitt et al., *Thromb. Haemost.* **92**, 419 (2004).
27. H. Umehara et al., *Arterioscler. Thromb. Vasc. Biol.* **24**, 34 (2004).
28. P. Lesnik, C. A. Haskell, I. F. Charo, *J. Clin. Invest.* **111**, 333 (2003).
29. We thank M. Sieweke (CIML, Marseille, France) and N. Hogg (Cancer Research UK, London, UK) for expert advice and the gift of reagents. We are also grateful to J. L. Casanova, P. Revy, B. Lucas, and S. Amigorena for expert advice and critical reading of the manuscript; C. Grolleau (Roper Scientific, Paris, France) for expert advice in the use of the Metamorph Software; Jennifer Wong for help in setting up the imaging of mesenteric vessels; and all the members of INSERM U838 for discussion and support. C.A. was a fellow of the Fondation de France. This work was supported by grants (to F.G.) from the Fondation Schlumberger, the Agence Nationale de la Recherche (grant IRAP2005), the City of Paris, the Fondation de France, the Fondation pour la Recherche Médicale, and a European Young Investigator award.

Regulation of Homeostatic Chemokine Expression and Cell Trafficking During Immune Responses

Scott N. Mueller,[1]* Karoline A. Hosiawa-Meagher,[2] Bogumila T. Konieczny,[1] Brandon M. Sullivan,[3] Martin F. Bachmann,[4] Richard M. Locksley,[3] Rafi Ahmed,[1] Mehrdad Matloubian[2]

The chemokines CCL21 and CXCL13 are immune factors that dictate homing and motility of lymphocytes and dendritic cells in lymphoid tissues. However, the means by which these chemokines are regulated and how they influence cell trafficking during immune responses remain unclear. We show that CCL21 and CXCL13 are transiently down-regulated within lymphoid tissues during immune responses by a mechanism controlled by the cytokine interferon-γ. This modulation was found to alter the localization of lymphocytes and dendritic cells within responding lymphoid tissues. As a consequence, priming of T cell responses to a second distinct pathogen after chemokine modulation became impaired. We propose that this transient chemokine modulation may help orchestrate local cellularity, thus minimizing competition for space and resources in activated lymphoid tissues.

A cardinal property of cells of the immune system is mobility, allowing them to navigate the body and combat invading pathogens. This is modulated by a complex array of chemokines and their receptors, which provide the molecular signals to direct cells to where they are required (1). Many chemokines are up-regulated in cells and tissues in response to inflammatory stimuli such as infection (2). In contrast, the lymphoid chemokines CCL21, CCL19, and CXCL13 are constitutively expressed in restricted areas for steady-state attraction of cells (3). CCL21 expression by fibroblastic reticular cells (FRCs) of the T cell zones in the spleen and lymph nodes (LN) facilitates effective interaction between dendritic cells (DCs) and T cells, whereas CXCL13 expression on follicular dendritic cells guides B cells and follicular T helper (T_H) cells into B cell zones (4, 5). The critical role of these homeostatic chemokines in attracting cells into lymphoid organs and in initiating antigen-specific responses is well established (3, 6). However, less is known about the impact that acute immune responses have on the expression of homeostatic chemokines and how this affects lymphocyte trafficking within lymphoid tissues.

[1]Emory Vaccine Center and Department of Microbiology and Immunology, Emory University School of Medicine, Atlanta, GA 30322, USA. [2]Department of Medicine, Division of Rheumatology, University of California, San Francisco, CA 94143, USA. [3]Howard Hughes Medical Institute and Department of Medicine and Department of Microbiology and Immunology, University of California, San Francisco, CA 94143, USA. [4]Cytos Biotechnology AG, Wagisstrasse 25, 8952 Schlieren, Switzerland.

*To whom correspondence should be addressed. E-mail: mueller@microbio.emory.edu